OFFICE OF CIVILIAN RADIOACTIVE WASTE MANAGEMENT
SPECIAL INSTRUCTION SHEET

1. QA: N/A

Page: 1 of: 1

Complete Only Applicable Items

This is a placeholder page for records that cannot be scanned.

2. Record Date	3. Accession Number
12/19/01	MOL.20020304.0040
4. Author Name(s)	**5. Author Organization**
YUETING CHEN	DUKE ENGINEERING & SERVICES

6. Title/Description
USING REACTIVE TRANSPORT MODELING TO EVALUATE THE SOURCE TERM AT YUCCA MOUNTAIN

7. Document Number(s)	8. Version Designator
N/A	N/A
9. Document Type	**10. Medium**
REPORT	OPTIC/PAPER

11. Access Control Code
PUB

12. Traceability Designator
RPR 30584; DC 30584

13. Comments
THIS ONE OF A KIND GREY SCALE DOCUMENT CAN BE LOCATED THROUGH THE RECORDS PROCESSING CENTER

QA:NA
DC#30584
12/19/01

Using Reactive Transport Modeling to Evaluate the Source Term at Yucca Mountain

Yueting Chen
Duke Engineering & Services
1180 Town Center Drive, Las Vegas, NV 89144, USA
yueting_chen@ymp.gov

Abstract

The conventional approach of source-term evaluation for performance assessment of nuclear waste repositories uses speciation-solubility modeling tools and assumes pure phases of radioelements control their solubility. This assumption may not reflect reality, as most radioelements (except for U) may not form their own pure phases. As a result, solubility limits predicted using the conventional approach are several orders of magnitude higher then the concentrations of radioelements measured in spent fuel dissolution experiments. This paper presents the author's attempt of using a non-conventional approach to evaluate source term of radionuclide release for Yucca Mountain.

Based on the general reactive-transport code AREST-CT, a model for spent fuel dissolution and secondary phase precipitation has been constructed. The model accounts for both equilibrium and kinetic reactions. Its predictions have been compared against laboratory experiments and natural analogues. It is found that without calibrations, the simulated results match laboratory and field observations very well in many aspects. More important is the fact that no contradictions between them have been found. This provides confidence in the predictive power of the model.

Based on the concept of Np incorporated into uranyl minerals, the model not only predicts a lower Np source-term than that given by conventional Np solubility models, but also produces results which are consistent with laboratory measurements and observations. Moreover, two hypotheses, whether Np enters tertiary uranyl minerals or not, have been tested by

comparing model predictions against laboratory observations, the results favor the former. It is concluded that this non-conventional approach of source term evaluation not only eliminates over-conservatism in conventional solubility approach to some extent, but also gives a realistic representation of the system of interest, which is a prerequisite for truly understanding the long-term behavior of the proposed repository. Therefore, it is a very promising alternative approach for source-term evaluation.

Key Words: reactive-transport modeling; nuclear waste; spent nuclear fuel; radionuclide solubility

1. Introduction

Geological disposal is being considered by several countries for nuclear wastes accumulated through power generation and other sources. An important aspect in assessing the performance of a potential nuclear waste repository is to evaluate the releases of radioactive elements from waste packages. Conventionally, they are capped by their solubility limits under the expected environments.

Solubility limits are usually estimated from geochemical modeling calculations, using speciation-solubility models, such as EQ3/6 (Wolery, 1992), PHREEQC (Parkhurst and Appelo, 1999), with supporting evidence from laboratory experiments (see e.g., Lemire and Garisto (1989), Bruno et al. (1997), Stockman and Moore (1999), Chen et al. (2000)). Typically, a pure-phase solid is chosen to control dissolved levels of each element of interest based on either laboratory and/or field observations or on conservative assumptions under the expected environmental conditions.

While the conventional approach described above has been a standard practice in the nuclear waste management community for over two decades, its shortcomings are also obvious. For instance, it is well recognized that the concentrations of most radionuclides in the process of spent fuel dissolution are likely to be very low (except for U) so that they may not form their

own pure phases (Grenthe, 1991; Langmuir, 1997). As a result, the predicted radionuclide solubility limits by the conventional approach may not match the concentrations measured in spent fuel dissolution experiments. The difference between them can be as high as several orders of magnitude, with the predicted values higher than the measured ones. A particularly important example of this is Np solubility.

Np is one of the most important actinides in nuclear waste disposal due to its long half-life and high dose-converting factor. The conventional solubility approach for Np usually assumes Np_2O_5 or other pure Np solids as the solubility-controlling mineral for Np. However, no Np pure phase has been identified in spent fuel dissolution experiments (Wilson, 1990a; Wilson, 1990b; Finch, 2000). The predicted Np solubility given by pure Np-solid models are several (3-7) orders of magnitude higher than the measured Np concentration in spent fuel dissolution experiments (Wilson and Bruton, 1990; Sassani and Siegmann, 1998; Chen, 2001).

The shortcomings of conventional solubility approach calls for innovative approaches to evaluate radionuclide source term. Several attempts have been reported along that direction (Sassani and Siegmann, 1998; Bruno et al., 1998; Murphy and Codall, 1999). On the other hand, as a new class of geochemical modeling tools – reactive-transport models - has fledged in the past two decades (Lichtner, 1985; Ortoleva et al., 1987; Yeh and Tripathi, 1991; Steefel and Lasaga, 1994; Chen, 1994; Parkhurst and Appelo, 1999). This also motivates geochemists to employ new geochemical modeling approaches to solubility evaluations. This study presents the author's attempt of applying the reactive-transport modeling approach to evaluate radionuclide release rates for a potential geological repository at Yucca Mountain Southern Nevada, USA.

2. Governing Equations and the Modeling Tool

2.1 Governing Equations

When both fluid flow and chemical reactions are considered, the concentration of aqueous species in porous media can be described by the mass conservation equation:

$$\frac{\partial \phi \rho_l \theta_l c_i}{\partial t} = -\nabla \cdot \vec{\mathbf{q}}_i + \sum_{k=1}^{N_r} \nu_{ik} W_k(\vec{\mathbf{C}}), \; i = 1, 2, \ldots, \mathrm{N_s} \tag{1}$$

where ϕ is porosity, ρ_l is the density of fluid, θ_l is the volumetric water content, c_i is the molal concentration of aqueous species i, and t is time. The first term on the right-hand side represents the contribution of transport processes to the change rate of c_i, where $\vec{\mathbf{q}}_i$ is the transport flux of species i. The second term on the right hand side represents the source/sink term of species i due to all chemical reactions (from reaction 1 to N_r), which in general is a nonlinear function of all concentrations $\vec{\mathbf{C}} = (C_1, C_2, \ldots, C_{N_s})^T$, where N_s is the total number of aqueous species; the superscript T denotes the transpose of the concentration vector; ν_{ik} is the stoichiometric coefficient of species i in reaction k, and W_k is the rate of reaction k.

If advection, dispersion, and diffusion are the transport processes to be included in $\vec{\mathbf{q}}_i$, and we assume that dispersion can be represented by a Fickian-type law, then

$$\vec{\mathbf{q}}_i = \phi \rho_l \theta_l (\vec{\mathbf{u}} c_i - \mathbf{D}_i(\theta_l) \cdot \nabla c_i) \tag{2}$$

where $\vec{\mathbf{u}}$ is the pore-water velocity; and $\mathbf{D}_i$ is the hydrodynamic dispersion tensor.

The source/sink term in Eq. (1) can be divided into two terms, one for equilibrium reactions, and the other for kinetic reactions:

$$\sum_{l=1}^{N_e} \nu_{il} W_l^e(\vec{\mathbf{C}}) + \sum_{j=1}^{N_k} \nu_{ij} W_j^k(\vec{\mathbf{C}}) \tag{3}$$

where W_l^e is the rate of equilibrium reaction l, while W_j^k is the rate of kinetic reaction j; N_e is the total number of equilibrium reactions (which will be eliminated by linear transformation upon Eq. (4), and thus, need not be defined); N_k is the total number of kinetic reactions; and $N_e + N_k = N_r$. This distinction has important consequences both for the capability of the model

(i.e., the capability to model both kinetic and equilibrium reactions) and for the numerical algorithms (i.e., the non-linear PDE of Eq. (1) cannot be reduced to linear PDEs if kinetic reactions are considered). Thus, the mass balance equation of solutes is

$$\frac{\partial \phi \rho_l \theta_l c_i}{\partial t} = -\nabla \cdot \phi \rho_l \theta_l [\vec{\mathbf{u}} c_i - \mathbf{D}_i(\theta_l) \cdot \nabla c_i] + \sum_{l=1}^{N_e} \nu_{il} W_l^e(\vec{\mathbf{C}}) + \sum_{j=1}^{N_k} \nu_{ij} W_j^k(\vec{\mathbf{C}}) \tag{4}$$

Rates of heterogeneous reactions can be parameterized as:

$$W_j^k = A_{m(j)} k_j \left[\prod_{\nu_{ij}<0} (a_i)^{|\nu_{ij}|/f_j} - \prod_{\nu_{ij}>0} (a_i)^{\nu_{ij}/f_j} / (K_j^{eq})^{1/f_j} \right] \tag{5}$$

where $A_{m(j)}$ is the effective reaction area in unit bulk volume, k_j and K_j^{eq} are rate constants and equilibrium constants, respectively; a_i is the activity of species i; f_j is the factor of reaction order.

The other aspect of reactive-transport modeling is the property of the rock matrix, as chemical reactions change not only the concentrations of solutes, but also the properties of rock matrix. For mineral m of spherical shape with a radius R_m, its volume fraction is given by

$$V_m = \frac{4}{3} \pi R_m^3 n_m \tag{6}$$

and its change rate is

$$\frac{\partial V_m}{\partial t} = 4\pi R_m^2 n_m \frac{\partial R_m}{\partial t} \tag{7}$$

where n_m is the number of grains of mineral m in unit bulk volume.

The dissolution rate of mineral m is the sum over all the dissolution/precipitation reactions pertaining to mineral *m*:

$$\frac{\partial R_m}{\partial t} = \sum_j k_j \left[\prod_{\nu_{ij}<0} a_i^{|\nu_{ij}|/f_j} - \prod_{\nu_{ij}>0} a_i^{\nu_{ij}/f_j} / (K_j^{eq})^{1/f_j} \right] / \rho_m \tag{8}$$

where ρ_m is the molar density of mineral *m* ([mol/L^3]).

2.2 The Modeling Tool – AREST-CT

The modeling tool used for this study is the general reactive-transport simulator AREST-CT (Chen et al., 1995; Chen et al., 1996; Chen et al., 1997; Chen, 1998) built on the governing equation system described in Section 2.1. The following physical-chemical processes are accounted for: 1) kinetic dissolution/precipitation of solid phases, 2) aqueous equilibrium speciation, 3) gas-aqueous equilibria, 4) redox reactions, 5) advection, 6) diffusion, 7) dispersion, and 8) nucleation thresholds for precipitation of new solids.

The simulator has the following features: 1) 1-D or 2-D simulation domains, 2) general interface to input user defined chemistry, 3) non-isothermal or isothermal chemistry, 4) ionic strength correction using the modified B-dot equation (Wolery, 1992), 5) spatially varying distribution of solid phases, and 6) effective reaction surface area depending on texture of solids.

The primary output of AREST-CT consists of: 1) concentrations of aqueous species and components as a function of time and space; 2) pH changes; 3) radii, surface areas, and volume fractions of solids; 4) dissolution/precipitation rates of solids; and 5) porosity changes.

AREST-CT utilizes a fully coupled numerical algorithm to solve the non-linear reactive-transport equations (Chen, 1994). The code was written in FORTRAN-77 and has been ported to various UNIX workstations.

3. Model Configurations

Under the current design, the potential repository would be located in tuffaceous units formed between 14 to 7.5 million years ago. The waste emplacement drafts would sit in an unsaturated zone and waste packages loaded with civilian spent nuclear fuel (CSNF) would be placed in them, as shown in Fig. 1. The current design also has a drip shield to protect the waste packages from ambient moisture.

Once a waste package and its drip shield fail, water may seep into it and react with CSNF. The model treats a CSNF waste package as a 1-D porous medium column, as shown in Fig. 2. The length of the column is 1.56 m, the inner diameters of a typical waste package. Dripping water enters the column at the top and exits it at the bottom. The volume fraction of CSNF is 14%, equal to the volume of CSNF in a waste package divided by the volume of the waste package. Cladding and basket materials occupy 21% of the space and are assumed chemically inactive for this study. Thus, the porosity of a waste package is 65%. The specific surface area of spent fuel was set to 39 cm^2/g, according to Gray and Wilson (1995). According to the modeling results for the long-term average seepage into drift (Francis et al., 1998), the velocity of water seeping into waste packages is set to 3.2 cm/year, water saturation in waste packages is set to be a constant 70%. The temperature is set to 90°C to match ANL's drip tests.

The composition of incoming water is listed in Table 1. Table 1 also gives the fugacities of $O_2(g)$ and $CO_2(g)$, according to in-drift chemistry modeling results (Sassani et al., 1998). Twenty-seven aqueous equilibrium reactions and two gaseous-aqueous equilibrium reactions were considered in the model, as listed in Table 2. All the equilibrium constants used in this study are from EQ3/6 database (Wolery 1992), unless stated otherwise.

Chemically, spent fuel is treated as pure UO_2. The reaction of spent fuel dissolution is given in Table 3. The equilibrium constant of uraninite (UO_2) is assigned to spent fuel. The dissolution of spent fuel is treated as a kinetically controlled. Gray et al. (1992) gives a rate law of CSNF based on flow-through dissolution experiments as:

$$\log R = 7.45 + 0.258 \log[C] + 0.142 \log[H^+] - 1550/T \qquad (9)$$

where R is the dissolution rate of U ($mg/[m^2\text{-day}]$), C stands for the total of CO_3^{2-} and HCO_3^-

concentrations (mol/kg), [H] stands for the concentration of H^+ (mol/kg), and T is the temperature in Kelvin. In AREST-CT, the UO_2 forward dissolution rate is implemented as:

$$R' = 0.00137 \times e^{-\frac{29697}{RT}} a_{\sum CO_3^{2-}}^{0.258} a_{H^+}^{0.142} \qquad (10)$$

where R' is the dissolution rate of spent fuel in [mol/m^2-sec], R is the gas constant, $a_{\sum CO_3^{2-}}$ and a_{H^+} are activities of [HCO_3^- +CO_3^{2-}] and H^+, respectively.

Nine secondary uranyl minerals have been identified as products of CSNF dissolution in drip-tests (Wronkiewicz et al., 1992; Finn et al., 1994; Finn et al., 1998). Similar uranyl mineral assemblages are observed at the natural analog site of Pena Blanca (Pearcy et al., 1994). The secondary uranyl minerals can be grouped into three categories: (a) uranyl-oxide hydrates, including schoepite, dehydrated schoepite, compreignacite, and becquerelite; (b) uranyl silicate hydrates: soddyite; and (c) uranyl alkaline silicate hydrates, including uranophane, boltwoodite, Na-boltwoodite, and sklodowskite.

In this study, four of these minerals, schoepite, soddyite, uranophane, and Na-boltwoodite are included in the model. The first two represent category (a) and (b), respectively, and the last two represent category (c). The dissolution/precipitation reactions for these minerals are given in Table 3. The rate constants for these mineral reactions were derived from the experimental results reported by Bruno et al. (1995), and Perez et al. (1997, 2000). They were derived by assuming the forward dissolution rate equals:

$$R = k_0 a_{H^+}^{\nu_{H+}} \qquad (11)$$

where ν_{H^+} is the stoichiometric coefficient of H^+ in the dissolution reaction for the mineral. Using the pH conditions of the experiment, the value of k_0 can be derived. Table 4 lists the

relevant rate constants. The rate constant for Na-boltwoodite is estimated based on the uranophane data, since they are similar in crystal structures and chemical compositions.

4. Simulation Results

The simulations were carried out for 10,000 years. Fig. 3 shows the calculated dissolution rate and volume changes of CSNF as a function of time and the position within a waste package. Fig. 3A shows that the dissolution rate of CSNF is almost constant, both spatially and temporally. Fig. 3B shows CSNF is almost totally consumed in about 100 years.

The development of secondary phases throughout the one-dimensional column of CSNF is shown in Fig. 4. Schoepite (Fig. 4A) is the major secondary uranyl-mineral and distributes almost uniformly within the waste package, except for the top portion (~0.1 m) of the waste package. In 100 years, about 30% schoepite (volume fraction of the WP) precipitates uniformly through the lower 1.4 m of the waste package, and another 5% schoepite accumulates after 100 years. The volume ratio of schoepite to the originally available spent fuel is about 35/14 = 2.50, which is very close to the expansion factor of molar volumes from UO_2 to schoepite (2.684). That means 93% of the original UO_2 is converted to schoepite. The rest has either formed uranophane or soddyite, or has been removed from the system by transport.

As shown in Fig. 4B, uranophane precipitates mainly in the top portion of the waste package. That is because the precipitation reaction rapidly depletes Ca and Si in the incoming water. For a similar reason, soddyite (Fig. 4C) precipitates at the top of waste package, due to the consumption of Si. Only trace amount of Na-boltwoodite was formed in the simulation (Fig. 4D).

Scrutinizing the development of the precipitation fronts of secondary minerals reveals that uranophane forms at the expense of schoepite and soddyite. Since the reactive-transport

model is based on the average of many solid grains and does not provide meaningful results for individual grains, the simulation results do not represent, in strict sense, the paragenetic sequence of secondary minerals. However, a general sequence of mineral formation can be derived from the movement of reaction fronts. Fig. 5 is the derived formation sequence of secondary minerals based on the simulation results. Stable phases are shown as solid lines and dashed lines represent meta-stable phases. Note that both schoepite and soddyite become meta-stable after spent fuel is consumed. As uranophane and soddyite replace schoepite, they are called tertiary minerals hereafter.

Fig. 6 shows the pH and U concentration (denoted as [U]) at the bottom of the waste package (exit) as functions of time. The pH drops initially and then reverses to its initial value, though the change is quite small (about 0.5 pH unit). [U] increases first and then decreases, due to the precipitation of secondary minerals. The final [U] at t = 1,000 years is about $3x10^{-5}$ mol/kg.

5. Model Validation

Model validation here indicates comparison of modeling results against data acquired from laboratory or field observations to evaluate the predictive capabilities of the model.

The laboratory and field observations used to do the comparison are the CSNF drip-tests reported by Wronkiewicz et al. (1992), Finn et al. (1994; 1998), and Pearcy (1994). The drip-tests are comparable with this model in several aspects: 1) both the model and experiments are flow-through system, 2) the composition of incoming water in both cases are J-13-like water reacted with tuff rock, and 3) the temperature is 90°C. Thus, the drip-tests are good benchmarks for validating the model. However, the comparison can be done only on semi-quantitative basis as, for example, the drip-tests are performed over much smaller scales in time and space.

The modeling results and corresponding experimental observations are listed side-by-side in Table 5, along with the author's comments/explanations. They are listed under four categories (i.e., the dissolution rate of CSNF, the abundance and distributions of secondary uranyl minerals, their paragenetic sequence, and the chemistry of water at the exit).

It should be pointed out that the simulation has not been calibrated by the laboratory and field observations. In other words, it is a blind prediction and no data have been manipulated. The only exception is that the observations of secondary mineral abundance have been utilized to make a choice of uranyl minerals to be included in the model.

The comparison given in Table 5 demonstrates that the model reproduces experimental results and field observations in many aspects. More important is the fact that no contradiction among them has been found yet. It strongly indicates that the model, consisting of the computer code, the conceptualization, and the data used in the simulation is a reasonably good representation of the real system.

The above validation shows the capability of the model in predicting the behaviors of CSNF under the repository conditions. The following section discusses the application of the model to predict the source terms, using Np as an example.

6. Source Term of Radionuclides - Np Concentrations at the Exit

CSNF contains a small amount of Np, depending on the fuel types, its burnout rate, and the time out of reactor. For example, the ATM-103 fuel contains about 0.00044 mole of Np for each mole of U. As CSNF dissolves, Np can be expected to do so as well:

$$\text{CSNF} + 2H^+ + 0.5\ O_2\ (g) = UO_2^{++} + 0.00044\ NpO_2^+ + H_2O \qquad (12)$$

Denoting the ratio of Np to U in solution as $(Np/U)_{soln}$ and in spent fuel as $(Np/U)_{fuel}$, we define the concentrating factor of Np, which measures the degree of Np being concentrated in solution compared to the spent fuel with which it is in contact, as

$$F_c = \frac{(Np/U)_{soln}}{(Np/U)_{fuel}} \qquad (13)$$

If all the Np released from the CSNF dissolution stays in solution, the concentration of Np and Fc should keep rising, as predicted by the simulation and as shown in Fig. 6. The simulation also predicts that Np concentration is as high as 1.0×10^{-5} mol/kg, which is three to four orders of magnitude higher than the measured Np concentrations in spent dissolution experiments (Finn et al., 1994; Wilson, 1990a; 1990b). This big difference indicates that Np was not totally released into solution during the process of fuel dissolution. Determining the mechanism(s) of Np retention is crucial to constraining Np concentration in performance assessment. Precipitation of Np pure phases is not considered since no such phases have ever been observed in spent fuel dissolution experiments.

Based on an analysis of the crystal-chemical properties of U-O bond, Np-O bond, and Pu-O bond, Burns et al. (1997) predict that "the substitutions $Pu^{6+} \leftrightarrow U^{6+}$ and $(Np^{5+}, Pu^{5+}) \leftrightarrow U^{6+}$ are likely to occur in most U^{6+} structures." Later, Buck et al. (1998) confirmed the prediction by finding Np incorporated into dehydrated schoepite. Therefore, it is reasonable to assume that during the process of CSNF dissolution some of the Np will be segregated into the secondary schoepite. Assuming Np enters schoepite with the same Np/U ratio as in the CSNF, then schoepite precipitation reaction would be:

$$UO_2^{2+} + 0.00044\ NpO_2^{+} + 3H_2O \Rightarrow \text{Np-bearing Schoepite} + 2H^{+} \qquad (14)$$

Although it is believed that Np can also be incorporated into tertiary uranyl minerals, such as uranophane, soddyite etc. (Burns et al., 1997), it is yet to be confirmed by laboratory

analysis. Thus, two possible hypotheses are considered: Hypothesis-1 assumes that Np does not incorporate into tertiary minerals and Hypothesis-2 assumes that Np incorporates into tertiary minerals congruently with U. For example, in Case-1, the uranophane reaction is

$$Ca^{++} + 2\ SiO_2(aq) + 2\ UO_2^{2+} + 4\ H_2O = \text{Uranophane} + 6\ H^+ \qquad (15)$$

while in Case-2, the reaction is:

$$Ca^{++} + 2\ SiO_2(aq) + 1.99912\ UO_2^{2+} + 0.00088\ NpO_2^{+} + 4\ H_2O = \text{Uranophane} + 6\ H^+ \quad (16)$$

Hypothesis-1 and Hypothesis-2 were implemented into the reactive-transport model of spent fuel dissolution described in Section 3, and the simulation results are presented in Fig. 7.

Fig. 7A shows [U], [Np], and F_c at the exit for Hypothesis-1. Over the period of 10,000 years, [Np] at the exit remains nearly constant of 1.0E-6 mol/kg. In contrast, [U] decreases with time. The steep decrease in [U] happens at about 100 years, when CSNF is totally consumed. Compared to the Np solubility (4.28E-5 mol/kg) predicted by Np_2O_5 model for comparable conditions, [Np] yielded by Hypothesis-1 is about 40 times lower. However, it is still about two orders of magnitude higher than Np concentration measured in spent fuel experiments (Finn et al., 1994; Wilson, 1990a, 1990b). On the other hand, over the same time period, F_c increases from less than 10 to over 100. The value and the trend of F_c do not match what have been observed in drip-tests (Chen, 2001), where F_c fluctuates around 1.0 and damps to 1.0 as time increases.

Fig. 7B is for Hypothesis-2. Like [U], [Np] decreases over the 10,000-years period, except for the very beginning. Before the disappearance of CSNF, [Np] is about 1.0E-7 mol/kg. After that, [Np] is about 1.0E-8 mol/kg. These values are closer to experimental measurements than that for Hypothesis-1. On the other hand, F_c remains constant of 1.0, which is consistent with laboratory observations (Chen, 2001).

Therefore, based on the comparison between the predicted and measured Np concentrations and time evolution patterns of F_c, it is reasonable to infer that Case-2 is more likely. In other words, Np incorporated not only into schoepite, but also into tertiary uranyl minerals is a better explanation for the observed Np concentrations and F_c behaviors with time in drip test.

7. Conclusions

A reactive-transport model for spent fuel dissolution and secondary phase precipitation has been constructed and validated by comparing modeling predictions against laboratory experiments and natural analogues. Based on the concept of Np incorporated into uranyl minerals, the model not only predicts a lower Np source-term than that given by conventional Np solubility models, but also produces results which are consistent with laboratory measurements and observations. Moreover, two hypotheses, whether Np enters tertiary uranyl minerals or not, have been tested by comparing model predictions against laboratory observations and the results favors Hypothesis-2. It is concluded that this non-conventional approach of source term evaluation not only eliminates some over-conservatism in conventional solubility approach, but also gives a realistic representation of the system of interest, which is a prerequisite for truly understanding the long-term behaviors of the proposed repository. Therefore, it is a very promising alternative approach for source-term evaluation

Acknowledgements-This work was supported by the U.S. Department Of Energy Yucca Mountain Site Characterization Office under contract #DE-AC08-01RW12101. The author would like to thank Patrick V. Brady for his review and Bechtel SAIC Company, LLC management for their support.

References

Bruno, J., Casas, I., Cera, E., Ewing, R.C., Finch, R.J., Werme, L.O., 1995. The assessment of the long-term evolution of the spent nuclear fuel matrix by kinetic, thermodynamic and spectroscopic studies of uranium minerals. Material Research Society (MRS) Symposium Proceedings 353, Pittsburgh, pp.633-639.

Bruno, J., Cera, E., de Pablo, J., Duro, L., Jordana, S., Savage, D., 1997, Determination of radionuclide solubility limits to be used in SR 97, Swedish Nuclear Fuel and Waste Management Co., Stockholm, Sweden, 184pp.

Bruno, J., Duro, L., de Pablo, J., Casas, I., Ayora, C. Delgado, J., Gimeno, M.J., Pena, J., Linklater, C., Villar, L.P., et al., 1998, Estimation of the concentrations of trace metals in natural systems. Chemical Geology, 151, pp.277-291.

Buck, E.C., Finch, R.J., Finn, P.A., Bates, J.K., 1998. Retention of neptunium in uranyl alteration phases formed during spent fuel corrosion. MRS Symposium Proceedings 506, Warrendale, Pennsylvania, pp. 87-94.

Burns, P.C., Ewing, R.C., Miller, M. L., 1997. Incorporation mechanisms of actinide elements into the structures of u^{6+} phases formed during the oxidation of spent nuclear fuel. Journal of Nuclear Materials, 245, pp.1-9.

Chen, Y., 1994. CIRF.A, A General, Coupled Reaction-Transport Model And Simulator. Ph.D. Dissertation, Indiana University, Bloomington, Indiana, 308pp.

Chen, Y., Engel, D. W., McGrail, B.P., Lessor, K.S., 1995. AREST-CT V1.0 Software Verification. Pacific Northwest Laboratories, Richland, Washington, 69pp.

Chen, Y., McGrail, B. P., Engel, D., 1996. A reaction-transport model and its application to performance assessment of nuclear waste disposal in Proceedings of International

Conference on Deep Geological Disposal of Radioactive Waste, Winnipeg, Manitoba, Canada, pp.8-21-8-30.

Chen, Y., McGrail, B.P, Engel. D. W., 1997. Source-term analysis for Hanford low-activity tank waste using the reaction-transport code AREST-CT. MRS Symposium Proceedings 506, Pittsburgh, pp. 1051-1058.

Chen. Y., 1998. Software Report for AREST-CT (Version 1.2), Civilian Radioactive Waste Management System Management and Operating Contractor (CRWMS M&O), Las Vegas, Nevada, 302pp.

Chen, Y., Lock, A., Wolery, T., Gaylord, R., Halsey, W., 2000, Summary of Dissolved Concentration Limits. CRWMS M&O, Las Vegas, Nevada, 167pp.

Chen, Y., 2001. An empirical Np solubility model based on spent fuel dissolution experiments, in Proceedings of the 9th International High-Level Radioacitve Waste Management Conference, Las Vegas, Nevada.

Finch, R., 2000. Secondary Uranium-Phase Paragenesis and Incorporation of Radionuclides into Secondary Phases. CRWMS M&O, Las Vegas, Nevada, 82pp.

Finn, P. A., Buck, E. C., Gong, M., Hoh, J.C., Emery, J.W., Hafenrichter, L.D., Bates, J.K., 1994. Colloidal products and actinide species in leachate from spent nuclear fuel. Radiochimica Acta, 66/67, pp.189-194.

Finn, P., Finch, R., Buck, E., Bates, J., 1998. Corrosion mechanism of spent fuel under oxidizing conditions. MRS Symposium Proceedings 506, Warrendale, Pennsylvania pp.123-131.

Francis, N.D., Itamura, M.T., Wilson, M.L., Grisak, G., Andrews, R.W., 1998. Total system performance assessment-viability assessment (TSPA-VA) analyses technical basis document - Thermal hydrology, CRWMS M&O, Las Vegas, Nevada, 658pp.

Gray, W., Leider, H., Steward, S., 1992. Parametric study of LWR spent fuel dissolution kinetics. Journal of Nuclear Materials, 190, pp.46-52.

Gray, W.J., Wilson, C.N., 1995. Spent Fuel Dissolution Studies FY 1991 to 1994. Pacific Northwest National Laboratory, Richland, Washington, 126pp.

Grenthe, I., 1991. Thermodynamics in migration chemistry. Radiochimica Acta, 52/53, pp.425-432.

Langmuir, D., 1997. Aqueous Environmental Geochemistry, Prentice Hall, New Jersey, 600pp.

Lemire, R., Garisto, F., 1989. The Solubility of U, Np, Pu, and Tc in a Geological Disposal Vault for Used Nuclear Fuel, Whiteshell Nuclear Research Establishment, Pinawa, Manitoba, Canada, 123pp.

Lichtner, P.C., 1985. Continuum model for simultaneous chemical reactions and mass transport in hydrothermal systems, Geochemica et Cosmochimica Acta, 49, 779-800.

Murphy, W.M., Codell, R.B., 1999. Alternate source term models for Yucca Mountain performance assessment based on natural analog data and secondary mineral solubility, MRS Symposium Proceedings 556, Pittsburgh, pp.551-558.

Nguyen, S.N., Silva, R.J., Weed, H.C., Andrews Jr., J.E., 1992. Standard Gibbs free energies of formation at the temperature 303.15 K of four uranyl silicates: soddyite, uranophane, sodium boltwoodite, and sodium weeksite. Journal of Chemical Thermodynamics, 24, pp.359-376.

Ortoleva, P., Chadam, J., Merino, E., Sen, A., 1987. Geochemical self-organization II: the reactive-infiltration instability, American Journal of Science, 287, pp.1008-1040.

Parkhurst, D.L., Appelo, C.A.J., 1999. User's Guid to PHREEQC (Version 2) – A Computer Program for Speciation, Batch-Reaction, One-Dimensional Transport, and Inverse Geochemical Calculations. US Geological Survey, Denver, 312pp.

Pearcy, E.C., Prikryl, J.D., Murphy, W.M., Leslie, B.W., 1994. Alteration of uraninite from the Nopal I Deposit, Pena Blanca District, Chihuahua, Mexica, compared to degradation of spent nuclear fuel in the proposed U.S. high-level nuclear waste repository at Yucca Mountain, Nevada. Applied Geochemistry, 9, pp.713-732.

Perez, I., Casas, I., Torrero, M., Cesa, E., Duro, L., Bruno, J., 1997. Dissolution studies of soddyite as a long-term analogue of the oxidative alteration of the spent nuclear fuel matrix. MRS Symposium Proceedings 465, Pittsburgh, pp. 565-572.

Perez, I., Casas, I., Martin, M., Bruno, J., 2000. The thermodynamics and kinetics of uranophane dissolution in bicarbonate test solutions. Geochimica et Cosmochimica Acta, 64(4), pp.603-608.

Sassani, D., Siegmann, E., 1998. Constraints on Solubility-Limited Neptunium Concentration for Use in Performance Assessment Analyses. CNWMS M&O, Las Vegas, Nevada, 26pp.

Sassani, D.C., Jolley, D.M., Chen, Y., Domski, P., Mariner, P., Stockman, C., 1998, Total system performance assessment-viability assessment (TSPA-VA) analyses technical basis document - near-field geochemical environment, CRWMS M&O, Las Vegas, Nevada, 417pp.

Steefel, C., Lasaga, A., 1994. A coupled model for transport of multiple chemical species and kinetic precipitation/dissolution reactions with application to reactive flow in single-phase hydrothermal systems. American Journal of Science, 294, pp.529-592.

Stockman, C., Moore, R., 1999, Use of dissolved and colloidal actinide parameters within the 1996 Waste Isolation Pilot Plant compliance certification application, in Reed et al., ed. Actinide Speciation in High Ionic Strength Media, Kluwer Academic/Plenum Publisher, New York, 1999, 271pp.

Wilson, C., Bruton, C., 1990, Studies on spent fuel dissolution behavior under yucca mountain repository conditions, in Nuclear Waste Management III, Ceramic Transaction 9, American Ceramic Society, pp.423-441.

Wilson, C.N. 1990a. Results from NNWSI Series 2 Bare Fuel Dissolution Tests. Pacific Northwest Laboratory, Richland, Washington, 92pp.

Wilson, C.N. 1990b. Results from NNWSI Series 3 Spent Fuel Dissolution Tests. Pacific Northwest Laboratory, Richland, Washington, 141pp.

Wolery. T.J., 1992. EQ3NR, A Computer Program for Geochemical Aqueous Speciation-Solubility Calculations: theoretical Manual, User's Guide, and Related Documentation. Lawrence Livermore National Laboratory, Livermore, California, 246pp.

Wronkiewicz, D., Bates, J., Gerding, T., Velechis, E., Tani. B., 1992. Uranium Release and secondary phase formation during unsaturated testing of UO2 at 90°C. Journal of Nuclear Materials, 190, pp.107-127.

Yeh, G.T., Tripathi, V.S., 1991, A model for simulating transport of reactive multispecies components: Model development and demonstration. Water Resource Research, 25, pp.93-108.

Fig. 1. Schematic of a waste placement draft.

Fig.2. Schematic of the simulation configurations. Water enters the waste package from the top, exits at the bottom, and reacts with SF while flows through it.

Fig. 3. Calculated CSNF volume (A) and dissolution rates of CSNF (B). The Y-axis is the depth into the column shown in Fig.1. 3A shows CSNF was totally consumed in about 100 years of dissolution. 3B shows the dissolution rate of CSNF varies less than 15% with time and space.

Fig. 4. Volume profiles of secondary minerals. (A) schoepite, the major secondary minerals, precipitates almost uniformly throughout the WP, except for the top portion; (B) uranophane precipitates mainly at the top of WP; (C) soddyite precipitates similarly to uranophane; (D) only trace amount of Na-boltwoodite precipitated.

Fig. 5. Paragenetic sequence of secondary uranyl minerals observed in the simulation results. Dashed line indicates meta-stable phases. Uranophane is the most stable uranyl mineral in the simulation.

Fig. 6. U(total) concentration, pH, Np(total) concentration, and concentrating factor (Fc) of Np at the exit as functions of time.

Fig. 7. U(total) concentration, Np(total) concentration, and concentrating factor (Fc) of Np at the exit as functions of time for Case-1 (A) and Case-2 (B).

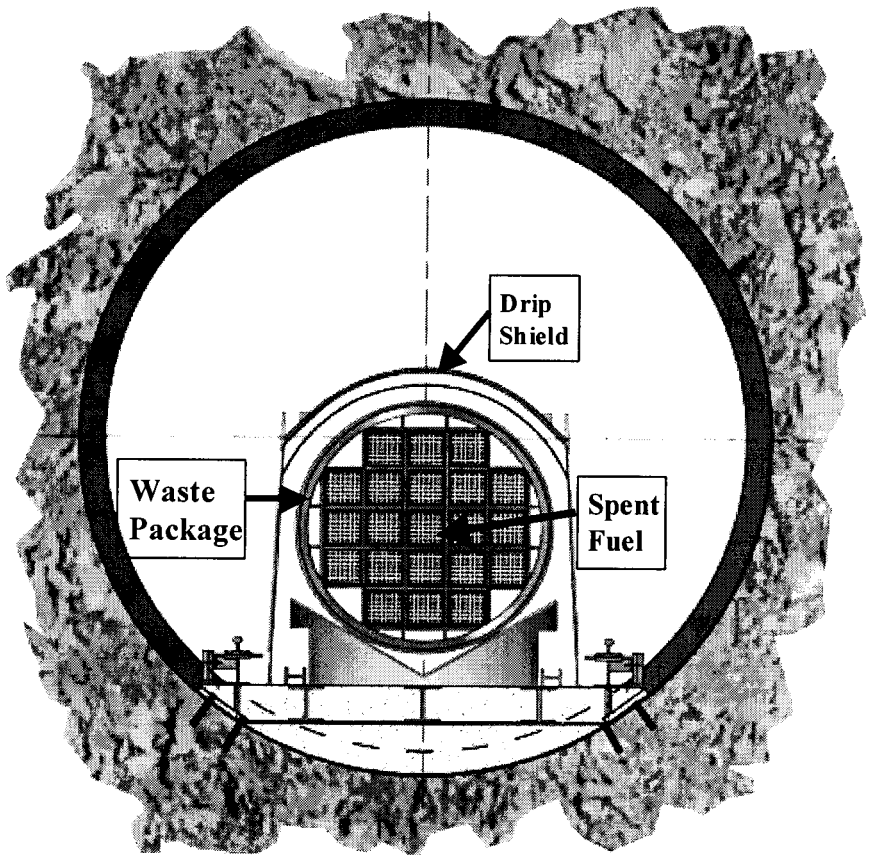

Fig. 1

Drawing Not To Scale

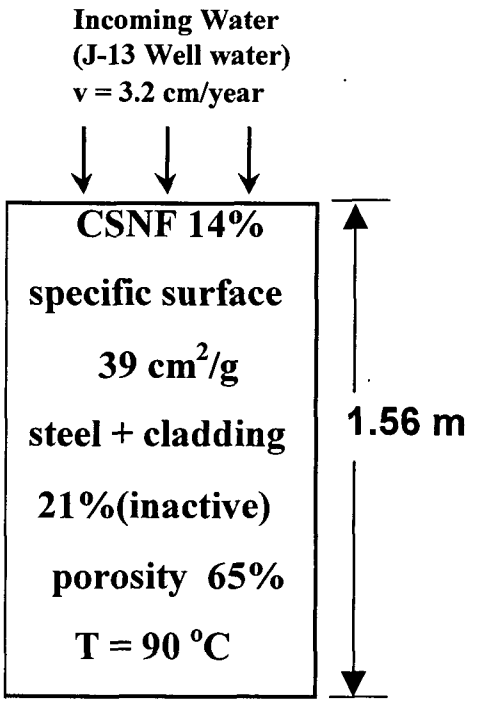
Incoming Water
(J-13 Well water)
v = 3.2 cm/year
CSNF 14%
specific surface
39 cm²/g
steel + cladding
21%(inactive)
porosity 65%
T = 90 °C
1.56 m

Fig. 2.

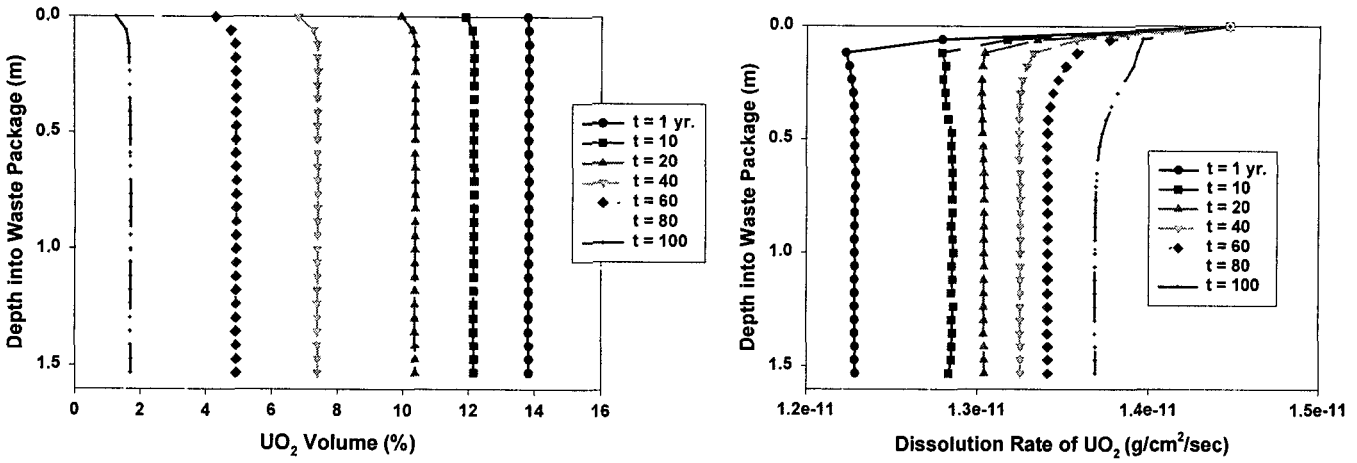
Depth into Waste Package (m)
0.0
0.5
1.0
1.5
0
2
4
6
8
10
12
14
16
UO2 Volume (%)
t = 1 yr.
t = 10
t = 20
t = 40
t = 60
t = 80
t = 100
Depth into Waste Package (m)
0.0
0.5
1.0
1.5
1.2e-11
1.3e-11
1.4e-11
1.5e-11
Dissolution Rate of UO2 (g/cm2/sec)
t = 1 yr.
t = 10
t = 20
t = 40
t = 60
t = 80
t = 100

Fig. 3A and 3B.

4A

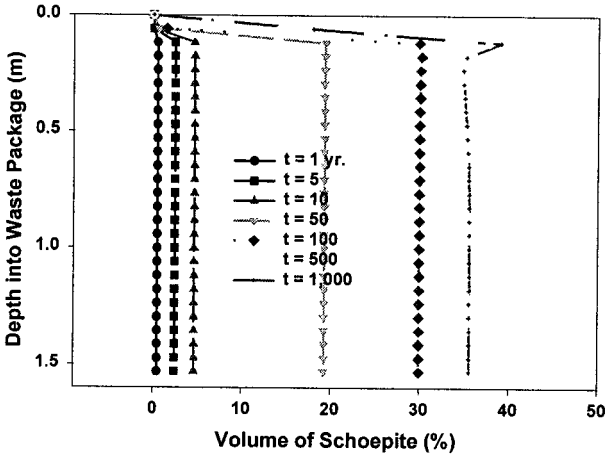

4B

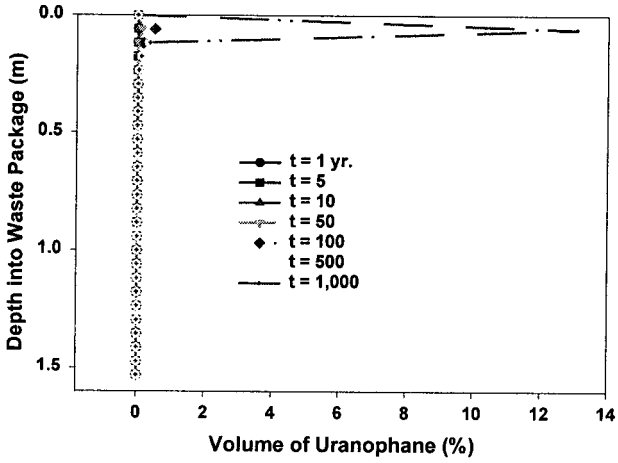

4C

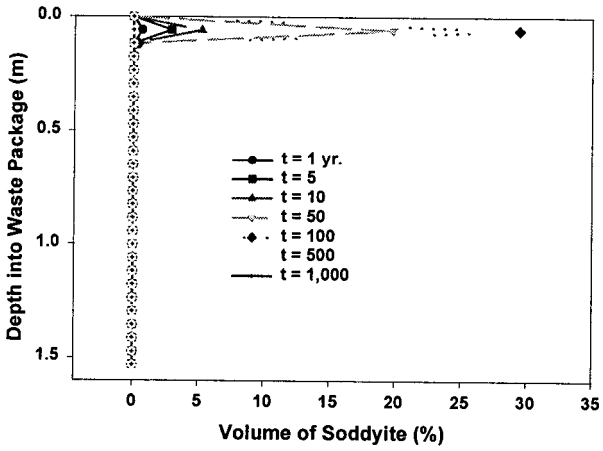

4D

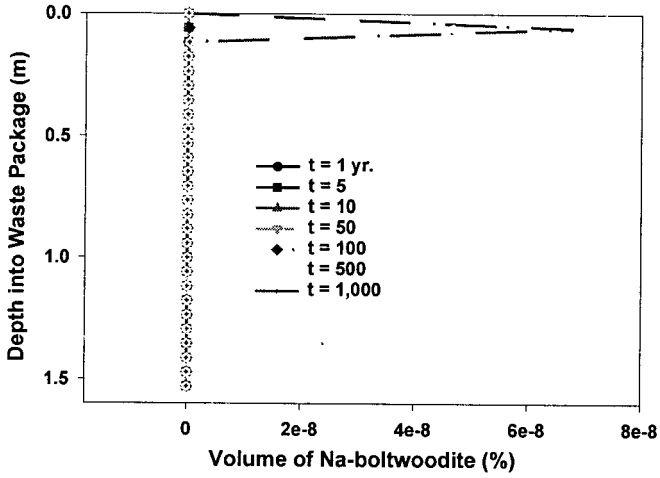

Fig. 4.

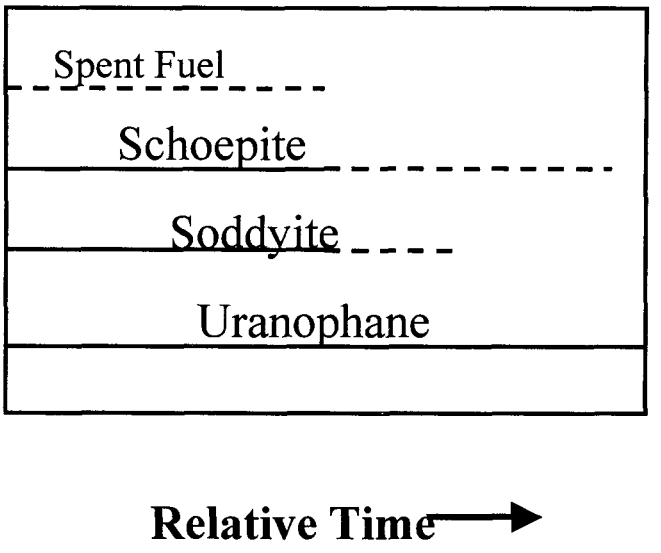

Fig. 5.

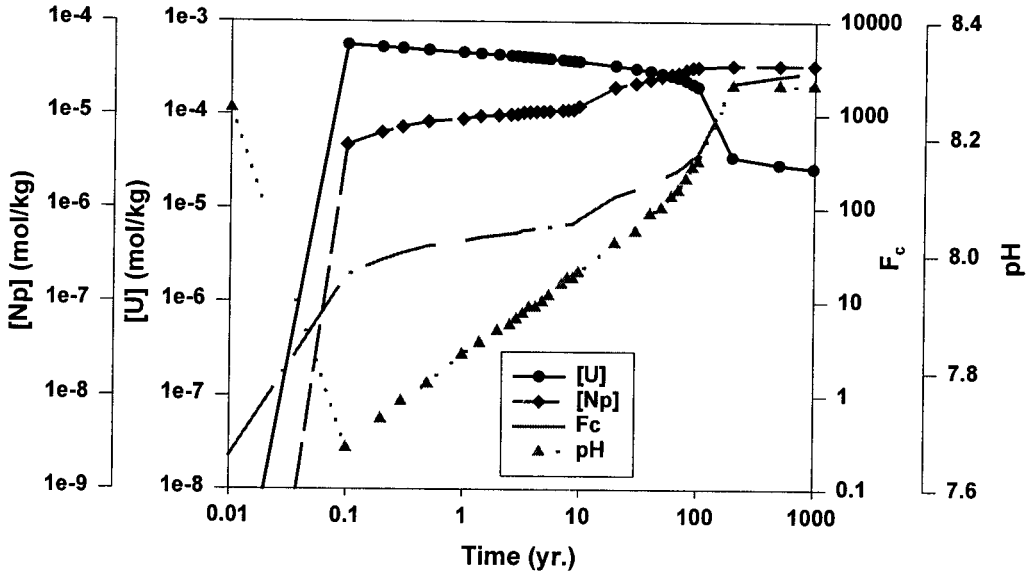
[Np] (mol/kg)
[U] (mol/kg)
F_c
pH
Time (yr.)
[U]
[Np]
Fc
pH
1e-4
1e-5
1e-6
1e-7
1e-8
1e-9
1e-3
1e-4
1e-5
1e-6
1e-7
1e-8
10000
1000
100
10
1
0.1
8.4
8.2
8.0
7.8
7.6
0.01
0.1
1
10
100
1000

Fig. 6.

7A

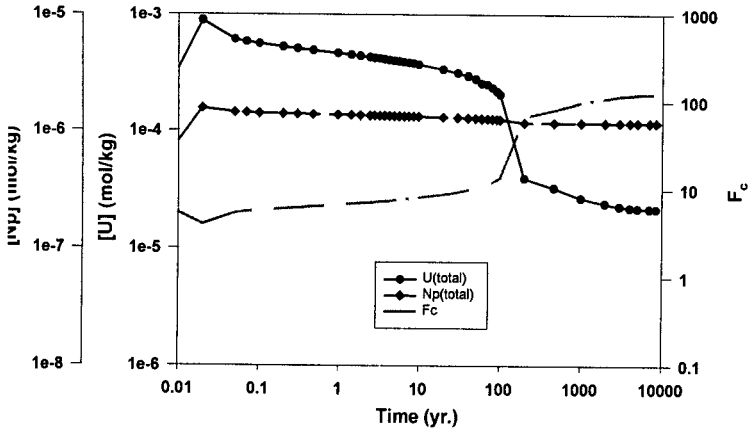
1e-5
1e-6
1e-7
1e-8
[Np] (mol/kg)
1e-3
1e-4
1e-5
1e-6
[U] (mol/kg)
1000
100
10
1
0.1
F_c
U(total)
Np(total)
Fc
0.01
0.1
1
10
100
1000
10000
Time (yr.)

7B

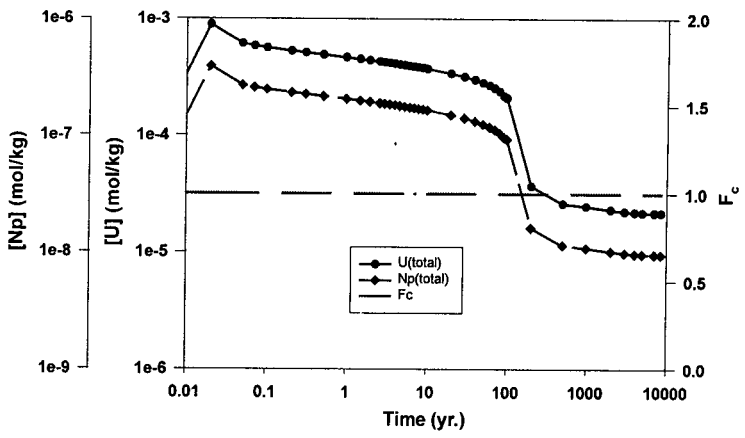
1e-6
1e-7
1e-8
1e-9
[Np] (mol/kg)
1e-3
1e-4
1e-5
1e-6
[U] (mol/kg)
2.0
1.5
1.0
0.5
0.0
F_c
U(total)
Np(total)
Fc
0.01
0.1
1
10
100
1000
10000
Time (yr.)

Fig. 7.

Table 1. Incoming Water Composition and Gas Fugacities

pH	8.25
Al (molality)	1.00E-8
K (molality)	1.29E-4
Mg (molality)	1.47E-7
Si (molality)	1.36E-3
Na (molality)	1.99E-3
Cl (molality)	2.01E-4
Ca (molality)	9.44E-5
U[a] (molality)	1.00E-10
Np[a] (molality)	1.00E-14
Logf_{CO2} (bars)	-3.0
Logf_{O2} (bars)	-0.7

[a] U and Np concentrations are arbitrarily assumed low.

Table 2. Equilibrium Reactions Considered in Simulations

Aqueous Equilibrium Reactions
$H_2O = H^+ + OH^-$
$CO_2(aq) + H_2O = H^+ + HCO_3^-$
$HCO_3^- = H^+ + CO_3^{--}$
$HSiO_3^- + H^+ = SiO_2(aq) + H_2O$
$CaCO_3(aq) + H^+ = Ca^{++} + HCO_3^-$
$CaHCO_3^+ = Ca^{++} + HCO_3^-$
$NaCO_3^- + H^+ = Na^+ + HCO_3^-$
$NaHCO_3(aq) = Na^+ + HCO_3^-$
$NaCl = Na^+ + Cl^-$
$NaHSiO_3(aq) + H^+ = Na^+ + SiO_2(aq) + H_2O$
$UO_2(CO_3)_3^{----} + 3H^+ = UO_2^{++} + 3\ HCO_3^-$
$UO_2(CO_3)_2^{--} + 2H^+ = UO_2^{++} + 2\ HCO_3^-$
$UO_2(CO_3)\ (aq) + H^+ = UO_2^{++} + HCO_3^-$
$UO_2(OH)_3^- + 3H^+ = UO_2^{++} + 3H_2O$
$UO_2(OH)_2\ (aq) + 2H^+ = UO_2^{++} + 2H_2O$
$UO_2(OH)^+ + H^+ = UO_2^{++} + H_2O$
$Np(OH)_{4(aq)} + H^+ = Np(OH)_3^+ + H_2O$
$Np(OH)_5^- + H^+ = Np(OH)_{4(aq)} + H_2O$
$NpO_2^{++} + 4\ H_2O = Np(OH)_5^- + 3H^+ + 0.5O_2(aq)$
$NpO_2(OH)^+ + H^+ = NpO_2^{++} + H_2O$
$NpO_2(CO_3)_2^{--} + 2H^+ = NpO_2^{++} + 2\ HCO_3^-$
$NpO_2(CO_3)_3^{----} + 3H^+ = NpO_2^{++} + 3\ HCO_3^-$
$NpO_2(OH)\ (aq) + H^+ = NpO_2^+ + H_2O$
$NpO_2(CO_3)^- + H^+ = NpO_2^+ + HCO_3^-$
$NpO_2(CO_3)_2^{---} + 2H^+ = NpO_2^+ + 2\ HCO_3^-$
$NpO_2^+ + 3.5\ H_2O = Np(OH)_5^- + 2H^+ + 0.25O_2(aq)$
$NpO_2(CO_3)_3^{-----} + 3H^+ = NpO_2^+ + 3\ HCO_3^-$
Gaseous-Aqueous Equilibrium Reactions
$CO_2(g) + H_2O = H^+ + HCO_3^-$
$O_2(g) = O_2(aq)$

Table 3. Solid Reactions

Solid	Reaction	Log K^{eq} Source
Spent Fuel UO_2	$UO_2 + 2\ H^+ + 0.5\ O_2(g) = UO_2^{++} + H_2O$	(Uraninite) EQ3/6
Uranophane $Ca(UO_2)_2(SiO_3)_2(OH)_2$	Uranophane + $6\ H^+ = Ca^{++} + 2\ SiO_2(aq) + 2\ UO_2^{++} + 4\ H_2O$	Nguyen et al., 1992
Schoepite $UO_3{:}2H_2O$	(Schoepite) + $2\ H^+ = UO_2^{++}\ 3\ H_2O$	EQ3/6
Soddyite: $(UO_2)_2(SiO_4){:}2H_2O$	Soddyite $+ 4\ H^+ = SiO_2(aq) + 2\ UO_2^{++} + 4\ H_2O$	Nguyen et al., 1992
Na-Boltwoodite $NaH_3OUO_2SiO_4{:}H_2O$	Na-Boltwoodite + $3\ H^+ = Na^+ + SiO_2(aq) + UO_2^{++} + 4H_2O$	Nguyen et al., 1992

Table 4. Rate Constants of Solid Dissolution

	Spent Fuel	Schoepite	Soddyite	*Uranophane*	Na-boltwoodite[a]
k_0 *(mol/m²-sec)*	0.00137	6.3E+6	6.8E+8	5.56E+35	2.0E+12
E_a *(J/mol)*	29697	0	0	0	0

[a] The rate constant for Na-boltwoodite is estimated based on the uranophane data.

Comparison of the Modeling Results and Observations

Phenomenon		Modeling Results	Lab Observations	Comments
Dissolution Rate of CSNF		The dissolution rate of spent fuel varies less than 15% with time and space.	"either that the reaction pathways have been constant during this time or that the contribution from multiple reaction pathways has not varied over time" (Finn et al., 1998)	The modeling results and laboratory observations match each other quite well.
		CSNF is totally consumed in about 1,000 years. In other words, more than 0.1% spent fuel dissolves each year.	"^{99}Tc release fraction should reflect the minimum matrix dissolution rate" (Finn et al., 1998) and "0.03 of the total ^{99}Tc inventory has been released after 3.7 years of reaction" (Finn et al. 1998) That is, 0.81% spent fuel dissolves each year	The predicted average dissolution rate of CSNF is of the same order of magnitude as the observed rate, but lower by a factor of 8. The lower dissolution rate in the simulation is caused by the lower temperature (70°C) used in the simulation.
Abundance and Distribution of secondary minerals	Schoe -pite	Schoepite is the major secondary phase and distributes evenly in the waste package.	"dehydrated schoepite is the dominant alteration phase" (Wronkiewicz et al., 1992)	The model calculation and laboratory observations match each other very well.
	Urano -hane	Uranophane mainly precipitated at the top of the WP.	"Uranophane is the most common phase observed on the top surface... but is conspicuously absent from the sides and bottoms of these samples" (Wronkiewicz et al., 1992)	The simulation correctly reproduces the same phenomenon observed in the experiments. They reflect the mechanism that the rapid precipitation of uranophane consumes Ca in the incoming water.
	Soddy -ite	a small amount (< 0.5%) of soddyite has been precipitated.	"Soddyite has been identified as a minor alteration product" (Wronkiewica et al., 1992)	The modeling result matches well with the lab observation.
Paragenetic Sequence		The paragenetic sequence of secondary uranyl phases is schoepite (uranium oxide hydrate)->soddyite->uranophane (uranium alkali solicate);	Wronkiewicz (et al., 1992) summarized the paragenetic sequence of drip-tests as uranium oxide hydrates->soddyite->uranium alkali silicate. Murphy. (1997) also gives a similar paragenetic sequence of uranyl minerals at the natural analog site at Pena Blanca	The good match in paragenetic sequence between simulation results and laboratory and field observations suggests that the model qualitatively reproduce the replacement relations among uranyl minerals.
Water Chemistry at Exit	pH	As shown in Fig. 5, the pH at the exit first decreases first and followed by an increase. The change is quite small, from 8.2 to 7.6;	"the pH (of the dripping water) was 8.4" (Finn et al., 1994) "the leachate had a pH of 6.0 at 57 d(ay) and 6.3 at 120 d" (Finn et al., 1994)	The simulation correctly reproduces the trend of pH changes, though the modeled change is smaller.
	U	Total concentration of U at the exit is between 10^{-5} –10^{-4} mol/kg.	The average U concentration of the leachate reported by Wronkiewicz (1992) is 3.2 μg/ml = 1.34×10^{-5} mol/kg.	The calculated U concentration matches the experiments very well.